Journal Name

Dynamic Article Links ►

Cite this: DOI: 10.1039/c0xx00000x

www.rsc.org/xxxxxx

ARTICLE TYPE

Study on Formation Mechanism and Ligand-directed Architectural Control of Nanoparticles Composed of Bi, Sb and Te: Toward One-pot Synthesis of Ternary $(Bi,Sb)_2Te_3$ Nanobuilding Blocks

Nguyen T. Mai, Derrick Mott, Nguyen T. B. Thuy, Issey Osaka and Shinya Maenosono*

Received (in XXX, XXX) Xth XXXXXXXXX 20XX, Accepted Xth XXXXXXXXX 20XX
DOI: 10.1039/b000000x

This paper reports a study on the formation mechanism of nanoparticles (NPs) composed of bismuth, antimony and tellurium for thermoelectric materials using a modified polyol synthetic route. Our one-pot synthesis technique has proven highly versatile in creating a wide range of different anisotropic NPs such as nanowires (NWs), nanodiscs (NDs), nanoribbons and nanospines (NDs studded on NWs) simply by modifying the capping species or elemental precursor feeding ratio used in the synthesis. However, an independent control of morphology and composition is still hugely challenging and the facile synthesis of $(Bi,Sb)_2Te_3$ solid solution NPs is not a trivial task, reflecting the complex nature of this multicomponent system. To achieve this goal, it is imperative to understand the formation mechanism based on a systematic investigation of mono- and binary elemental NP systems. Our study clearly shows the different actions of oleylamine (OAM) and decanethiol (DT) capping ligands in our synthesis reaction. In the case of DT capping system, Te NDs are first formed, and then, Bi and Sb are separately incorporated into the Te ND structure via catalytic decomposition of Bi-DT and Sb-DT complexes on the Te ND surfaces. Therefore, the resulting NPs are phase segregated into Te, Bi_2Te_3 and Sb_2Te_3. On the other hand, in the case of OAM capping system, Te NWs and Bi-Sb solid solution NPs are formed separately, and then, parts of Te NWs are transformed into $(Bi,Sb)_2Te_3$ phase via oriented attachment of Bi-Sb NPs and Te NWs. These findings are crucially important toward one-pot synthesis of uniform $(Bi,Sb)_2Te_3$ nanobuilding blocks with controllable characteristics for highly efficient thermoelectric materials.

Introduction

With the advent of nanotechnology the field of thermoelectric (TE) materials has been rejuvenated, and what was once thought of as an area of research with insurmountable challenges has now become one of the most promising technologies to extend our current energy sources.[1] TE materials are highly exciting because they exhibit the Seebeck effect which can be used to create devices that harvest excess heat to create electricity, or can be used to make freonless refrigerators, cool microelectronics, etc.[1,2] Nanoparticles (NPs) have proven useful in these materials because the small particle (grain) size causes scattering of the heat carrying phonon along the crystal boundaries, effectively allowing the thermal conductivity to be reduced while maintaining the electrical conductivity.[2,3] In addition, it has been demonstrated that the NP shape plays a key role in this effect because the orientation and area of the grain boundaries can be tuned by long range ordering of the NPs, for example superlattices of one-dimensional nanowires (NWs) or two-dimensional nanodiscs (NDs).[4-6] This causes the overall efficiency of the material to be increased, which is expressed by the dimensionless figure of merit, $ZT = \alpha^2\sigma T/\kappa$, where α is the Seebeck coefficient, σ is the electrical conductivity, κ is the thermal conductivity and T is the absolute temperature.[1] With this in mind, several researchers have attempted to create efficient TE materials with nanostructuring. Bi-Te alloy systems are known to have some of the highest ZT values at low temperature range (< 600 K).[2] By creating Bi-Te alloy based NPs, the thermoelectric efficiency is predicted to be even higher.[3,7,8]

Currently there is a large amount of attention being devoted to the creation of nanostructured TE materials. Most often, the synthetic approaches to the TE nanomaterials include techniques such as hydrothermal,[9] electrochemical deposition,[10-13] pulsed laser deposition,[14] sputtering,[15] shear extrusion,[16] mechanical alloying,[17] spark plasma sintering,[18] rapid solidification processes,[19] microwave assisted organic surfactant synthesis,[20,21] or sonoelectrochemistry.[22] Despite much attention being given to the creation of the nanostructured TE materials, few techniques have proven successful at the creation of true nanoscale particles with controllable size, shape and composition composed of Bi-Te alloys. In response to the challenges encountered in these preparation techniques, a few researchers have begun to explore wet chemical based synthesis techniques towards binary Bi-Te alloy NPs with controllable properties in terms of size, shape,

composition, etc. For example, the synthesis of well-defined Bi_2Te_3-Te heterogeneous nanostructures by controlling the kinetic reaction of Bi^{3+} and TeO_3^{2-} in the presence of hydrazine,[23] the inorganic surfactant assisted solvothermal synthesis of Bi_2Te_3 nanoplates,[24] the ligand-directed synthesis of Bi_2Te_3 nanorods or nanosheets,[25] or the hot injection synthesis of Bi_2Te_3 nanoplatelets in the presence of oleic acid[26] have been previously reported. Moreover, the synthesis of Bi_2Te_3 NPs through a microemulsion synthetic route,[27] two-step synthesis of Bi_2Te_3 NPs from Bi seeds in the presence of oleylamine,[28] hydrothermal synthesis of Bi_2Te_3 NWs through the solid state interdiffusion of Bi and Te,[29] surfactant directed synthesis of Bi_2Te_3/Bi_2S_3 core-shell nanorods,[30] and two-step synthesis of well-defined Bi_2Te_3 nanotubes based on solution phase nanoscale Kirkendall effect[31] have illustrated the feasibility of using chemically synthesized NPs to create materials with enhanced TE properties because of the highly controllable characteristics of the NPs.

The $(Bi,Sb)_2Te_3$ ternary solid solution system is known as a *p*-type TE material and has a higher *ZT* value when compared with the Bi_2Te_3 binary alloy.[32,33] This is mainly because $(Bi,Sb)_2Te_3$ exhibits significantly reduced lattice thermal conductivity due to increased unit cell size, low crystal symmetry, and site occupancy disorder. As stated above, chemical synthesis strategies for binary Bi_2Te_3 NPs have been somewhat successful, even though the formation mechanisms of those NPs have not been completely clarified yet. Meanwhile, however, there have been very few successful reports on the direct chemical synthesis of $(Bi,Sb)_2Te_3$ ternary solid solution NPs. For example, Talapin and co-workers have reported the formation of a $Bi_{2-x}Sb_xTe_3$ nanostructured thin film by annealing Bi_2S_3 nanorods functionalized with Sb_2Te_3 metal chalcogenide complex.[3] Zhao and co-workers synthesized nanocrystalline Bi-Sb-Te bulk solids by a combination of hydrothermal synthesis and hot pressing.[9] Ren and co-workers created irregular-shaped $(Bi,Sb)_2Te_3$ bulk solids in an aqueous-phase reduction process.[34] All of these synthetic approaches did not lead to isolated $(Bi,Sb)_2Te_3$ ternary solid solution NPs. Exceptionally, Burda and co-workers successfully synthesized isolated $Bi_{0.5}Sb_{1.5}Te_3$ angular shaped NPs by direct chemical solution synthesis. They first heated bismuth acetate $[Bi(OAc)_3]$ and antimony acetate $[Sb(OAc)_3]$ dissolved in phenylether in the presence of dodecanethiol (DDT) for 1 h followed by injection of Te dissolved in trioctylphosphine (TOP), followed by reaction for 30 minutes to form $Bi_{0.5}Sb_{1.5}Te_3$ NPs.[35] Weller and co-workers also reported the successful synthesis of isolated $Bi_xSb_{2-x}Te_3$ nanoplatelets[36] which was similar to the synthetic route of Burda and co-workers.[35] They first heated $Bi(OAc)_3$ and $Sb(OAc)_3$ dissolved in DDT for 45 min followed by injection of oleylamine and Te dissolved in TOP to form $Bi_xSb_{2-x}Te_3$ nanoplatelets.

The above mentioned synthetic techniques typically required multiple steps with the preparation of elemental precursors and lead to only one specific type of NP in terms of shape or structure, making these approaches very limited in the range of NPs they can produce. The polyol synthetic technique is one that has proven very versatile for synthesizing NPs with controllable size, shape, composition, and structure, and in our own research we have demonstrated that in a one-pot synthesis, this general approach can lead to a wide variety of Bi, Sb and Te based NPs with tunable shape and composition simply by changing the nature of the capping species used in the synthesis.[37] Because of the importance in synthesizing $(Bi,Sb)_2Te_3$ ternary solid solution NPs with controllable characteristics we present here a study on the formation mechanism of these promising nanoscale materials. The complexity associated with the formation mechanism of NPs is remarkably increased with the presence of more than one elemental precursor and capping ligand. Even in the single elemental system, the growth mechanism was reported to be not simply based on the function of surfactant as a soft template for NP growth.[38] Expanding to the double elemental NPs, not only the effect of surfactant but many other factors such as the relative reaction rate or the interaction of the two elemental precursors should be taken into account for the increased difficulties in elucidating the NP formation pathway.[39-42] Therefore, in a ternary system, there are many more challenges in addressing the formation mechanism without understanding of the fundamental formation of mono- and bi-elemental NPs. Our synthesized NPs consist of Bi, Sb and Te, which are in general considered to be a poor metal (Bi) or a semi-metal (Sb and Te) but hereafter are referred to as "metals". Hence, a systematic study of mono-, bi- and trimetallic NP synthesis is strongly required to investigate the formation mechanism in this complex system. Our results detail the effect of capping ligands, precursors and the metal-ligand cross interaction on NP morphology and composition and elucidate the different formation mechanisms that occur with different capping species. The formation and synthesis of ternary BiSbTe NW alloy in oleylamine and binary BiTe/SbTe NDs in decanethiol will be discussed.

Experimental Section

Chemicals

Bismuth trichloride ($BiCl_3$, purity 99%), antimony trichloride ($SbCl_3$, purity 99%), tellurium tetrachloride ($TeCl_4$, purity 99%), oleic acid (OAC, purity 90%), oleylamine (OAM, purity 70%), 1,2-hexadecanediol (HDD, purity 90%), 1-decanethiol (DT, purity 96%), 1-dodecanethiol (DDT, purity 98%) and dioctylether (purity 99%) were purchased from Sigma Aldrich Corp. as well as other common solvents. All reagents were used without further purification.

Synthesis of NPs

1.67×10^{-4} moles each of $BiCl_3$, $SbCl_3$ and $TeCl_4$ precursor were used in monometallic synthesis. For each bimetallic and trimetallic synthesis, a total 5×10^{-4} moles of elemental precursor was used with equimolar feeding ratio. Elemental precursors were mixed with 25 mL of dioctylether, and 1.5×10^{-3} moles of HDD was added along with the capping species, the identity of which was used to manipulate the morphology and composition of the resulting NPs. In this work, OAM, OAC/OAM and DT were used as capping agents with varying ratios and amounts. The exact amount of capping species used in each synthesis is described more fully in the text. Next, the mixture was purged with argon under vigorous stirring. At this point the reaction temperature was raised to 105 ºC for 10 minutes to remove water, which also caused the reactants to completely dissolve in the solvent (a light grey color in the solution). After this, the temperature was increased to 200 ºC and was held for 1 hour. The formation of particles within this time was evidenced by the

solution color change from light grey to dark grey or black depending on the capping species used. After reaction, the NP solution was cooled to room temperature and the particles were purified by precipitation in ethanol. The materials could be briefly resuspended in hexane with additional OAC, OAM and/or DT. The resulting NPs were then analyzed.

Instrumentation and analysis conditions

An array of instrumental techniques including X-ray diffraction (XRD), transmission electron microscopy (TEM), energy dispersive spectroscopy (EDS), inductively coupled plasma mass spectroscopy (ICP-MS), electrospray ionization Fourier transform ionization cyclotron resonance mass spectroscopy (ESI-FTICR-MS), and thermogravimetry (TG) were used to characterize the size, shape, composition, structure and other properties of the materials. XRD patterns were collected in reflection geometry using a Rigaku RINT2500 X-Ray diffractometer at room temperature with Cu Kα radiation (wavelength 1.542 Å). TEM analysis was performed on Hitachi H-7100 and H-7650 transmission electron microscopes operated at 100 kV. TEM samples were prepared by dropping the suspended particles onto a carbon coated copper grid and drying in air overnight. Samples for ICP-MS were prepared by dissolving in aqua regia then were diluted using nitric acid solution (2-5%). The data was collected using a Hitachi Plasma Mass Spectrometer P-5000 with guide voltages of 30, 35, and 50 V for Sb, Te, and Bi isotopes, respectively. A Fourier transform ion cyclotron resonance mass spectrometer equipped with a 9.4 T superconducting magnet (SolariX, Bruker Daltonics) was used to analyze the metal-ligand complex solution. TG analysis was performed using a Seiko TG/DTA6200. Samples underwent heat treatment from 25 to 600 ºC in flowing nitrogen gas with a heating rate of 10 ºC per minute.

Results and Discussion

In the previous work,[37] we successfully synthesized NPs composed of Bi, Sb and Te using different capping systems and the complexity that arose in the ternary alloy system inspired us to conduct a more systematic study to investigate the formation mechanism for controlling the morphology and composition of the final NPs. In this study, three capping systems consisting of OAM, OAC/OAM and DT were used to synthesize mono-, bi- and trimetallic NPs. We studied the effect of individual interaction between capping ligand and metal precursor on NP morphology and composition from the results of the primary synthesis using only one metal precursor with each capping system. Then the combination of two metal precursors was studied to clarify the role that each metal plays in the synthesis, along with effect of capping ligands in the reaction/incorporation of the two metals into the final NPs. These results together with the characterization of trimetallic NPs synthesized using each capping system help to clarify the formation mechanism of trimetallic NPs in these complex systems. As a result of the wide range of synthesis conducted with varying reaction conditions, not all of the synthesized materials have an ideal size, structure or composition. Many of the results related in this work show the formation of micro-sized particles, non-homogeneous structure/composition, or oxidized materials, etc., however these results still shed light on the underlying formation mechanism of NPs in this system. Additionally, it is also important to note that the three different capping ligands used in this study were not further purified before use, so a significant portion of these ligands (especially OAM) may include short alkane chain impurities. It is well known that trioctylphosphine oxide (TOPO) ligands contain impurities such as phosphonates and phosphonic acid, and these impurities may very well bind far more strongly to cation sites than TOPO. The ligands used in this study may also contain impurities which have different functional groups. While these impurities may influence the particle size or shape formation, this study primarily focuses on the chemical nature of the reactive terminus of the primary component of the ligands (i.e. amine, carboxylate and thiol), which is the primary factor leading to the various particle size, morphology, structure and compositions observed.

Table 1. Main products synthesized using a single metal precursor

Metal Precursors	Organic Capping Ligands		
	OAM	OAC/OAM	DT
$BiCl_3$	BiOCl aggregates	BiOCl aggregates	Bi plates D ~ 500 nm L > 2 μm
$SbCl_3$	Sb NWs D ~ 100 nm L ~ 2–10 μm	Sb NWs D ~ 100 nm L ~ 2–10 μm	No solid product
$TeCl_4$	Te NWs D ~ 200 nm L ~ 5–10 μm	Te NWs D ~ 100 nm L ~ 2–6 μm	Te nanoplates D ~ 100 nm

D and L represent mean diameter and length estimated from TEM images, respectively

Study of monometallic synthesis approach

Bi, Sb and Te monometallic NPs were synthesized using a single metal precursor with the various capping systems. The morphology and crystal structure of the resulting NPs were characterized by TEM and XRD analyses. The results are briefly summarized in Table 1.

Synthesis of Bi NPs

Figure 1 shows the XRD patterns (A-C) and TEM images (D and E) of materials synthesized using a $BiCl_3$ precursor. When OAM or OAC/OAM is used as a capping system, bismuth oxychloride (BiOCl) was mainly formed with elemental Bi with rhombohedral phase as a minor product as seen in Fig. 1A and B (for detail see Supplementary Information Tables S1 and S2). The BiOCl NPs are insoluble in any kind of solvent used in this study. The peak broadening in the XRD pattern indicates that the mean crystalline sizes of BiOCl and Bi are relatively small. Figure 1D shows a TEM image of the sample synthesized using OAM. Large aggregates composed of matrix having an indeterminate form and small NPs with spherical shape with a diameter of about 20 nm are observed. Similar TEM images were also observed for the case of using OAC/OAM (not shown). In consequence, we attribute the small spherical NPs and the matrix in Fig. 1D to Bi NPs and BiOCl crystals, respectively. It is well known that $BiCl_3$ reacts with water to give a white precipitate of BiOCl. The source of oxygen in the present syntheses may be residual water and/or oxygen molecules dissolved in the solvent (dioctylether) which could not be completely removed, even under argon purging and elevated temperature. In addition, it has also been reported that BiOCl was formed in the synthesis of Bi_2S_3 with $BiCl_3$ and sulfur

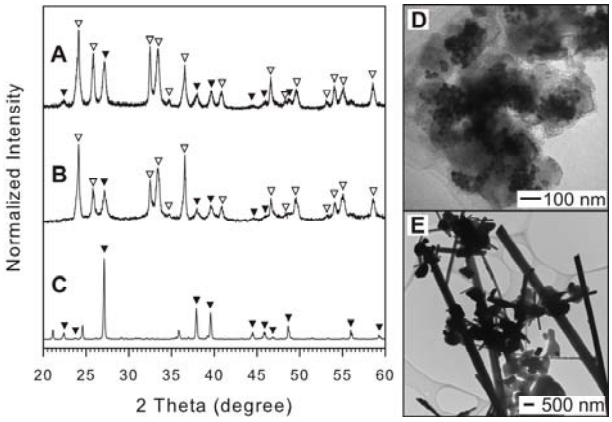

Fig. 1. XRD pattern and TEM images of materials synthesized using OAM (A and D), OAC/OAM (B), and DT (C and E). The indexed peaks are marked by the symbols open triangle (▽) for BiOCl (JCPDS card no. 006-0242) and filled triangle (▼) for Bi (JCPDS card no. 044-1246). For detailed peak position and assignment see Supplementary Information Tables S1-S3.

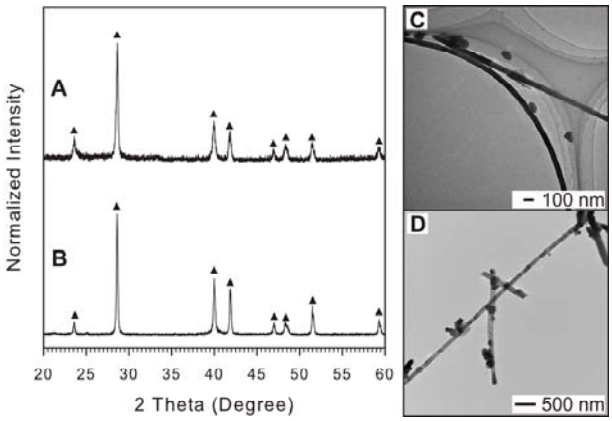

Fig. 2. XRD patterns and TEM images of Sb NWs synthesized using OAM (A and C) and OAC/OAM (B and D). In the case of using DT, no solid particles can be obtained. The upright filled triangles (▲) indicate peaks assigned to Sb with rhombohedral structure (JCPDS card no. 01-085-1322) in the XRD pattern (A and B) (for detail see Supplementary Information Tables S4 and S5).

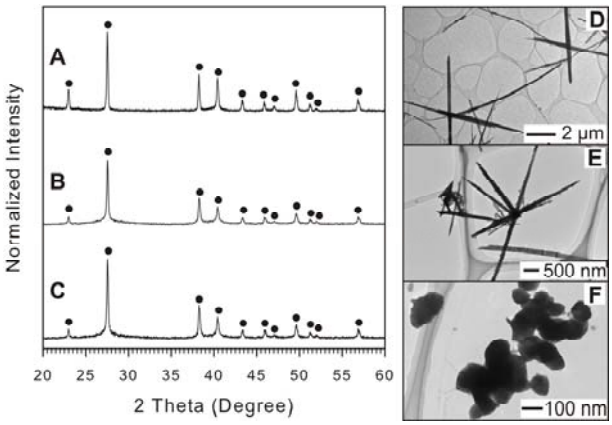

Fig. 3. XRD pattern and TEM images of resulting NPs synthesized using OAM (A and D), OAC/OAM (B and E), and DT (C and F). The XRD peaks are labeled by filled circle (●) for hexagonal structured Te (JCPDS card no. 036-1452). For detail, see Supplementary Information Tables S6-S8.

precursors using OAM as solvent and capping ligands even under a water-free environment[43] which is similar to our observation.

Changing to the DT capping system, only an elemental Bi phase was observed with some minor unidentifiable peaks (unlabeled) in the XRD pattern as shown in Fig. 1C. These minor peaks could arise as a result of some leftover bismuth precursor-ligand complex which could not be removed during the particle purification process. A mixture of elongated plate-like particles (~500 nm in diameter and several microns in length) and smaller polyhedral shaped particles (~500 nm) are shown in Fig. 1E. These results suggest that DT makes stable complexes with the Bi cation and protect it from creating BiOCl while OAC and OAM ligands do not.

Synthesis of Sb NPs

Similarly, syntheses with $SbCl_3$ and capping ligands OAM, OAC/OAM and DT were performed. Figure 2 shows the XRD patterns (A and B) and TEM images (C and D) of the synthesized NPs. When OAM or OAC/OAM is used as a capping system, the XRD patterns collected for the samples are well defined for elemental Sb with rhombohedral structure without by-product such as antimony oxychloride (SbOCl) as shown in Fig. 2A and B (for detailed peak positions and assignment see Supplementary Information Tables S4 and S5). Using OAM or OAC/OAM leads to the formation of NWs which have a diameter of about 100 nm and length of several microns (Figs. 2C, D, S1 and S2). However, using DT as a capping system, Sb was not successfully reduced under the reaction conditions as evidenced by the fact that the reaction solution did not change color during one hour of heating at 200 ºC and no solid materials could be obtained. This phenomenon can be explained due to the stable complex that Sb forms with DT which is not easily decomposed, preventing the subsequent reduction and formation of Sb NPs. To further probe the observation, the Sb-DT synthesis was also conducted at 240 ºC, which resulted in a brown suspension that quickly returned to a clear color upon cooling of the reaction. When the synthesis was repeated using dodecanethiol (DDT) at 250 ºC, an identical phenomenon was observed. The results indicate that Sb NPs could not be synthesized in the presence of DT or DDT, even at elevated temperature, perhaps because of an etching effect of Sb metal by thiol containing ligands.

In a separate experiment, $SbCl_3$ could be dissolved in DT and hexane solvent at room temperature (Supplementary Information Fig. S3) and ESI-FTICR-MS was used to detect high molecular weight fragments containing Sb isotopes coupled with an organic component which arises from the Sb-DT complex (Supplementary Information Fig. S4). Moreover, thermal analysis for the Sb-DT complex shows a slow mass loss taking place before 220 ºC (Supplementary Information Fig. S5) which explains the stability of the Sb-DT complex under the reaction conditions. The study of monometallic Sb synthesis suggests that different capping ligands created a complex with Sb with different stability in which DT makes a more stable complex that did not undergo the reduction to Sb NPs while OAM or OAC/OAM create a weaker complex that can be reduced to form elemental Sb NWs.

Synthesis of Te NPs

Figure 3 shows the XRD patterns (A-C) and TEM images (D-F) of NPs synthesized using $TeCl_4$ precursor. The composition and structure of all resulting NPs determined based on the indexed

Table 2. Main products synthesized using two different kinds of metal precursors

Metal Precursors	Organic Capping Ligands		
	OAM	OAC/OAM	DT
$BiCl_3$, $SbCl_3$	BiSb nanoplates D ~ 20–60 nm	BiSb NPs D ~ 20–40 nm	Bi plates D ~ 100–300 nm L ~ 10 μm
$BiCl_3$, $TeCl_4$	Te NWs D ~ 30–200 nm L ~ 3–10 μm	Te NWs D ~ 100–200 nm L ~ 3–10 μm	Bi-Te NDs D ~ 30–50 nm H ~ 5–10 nm
$SbCl_3$, $TeCl_4$	Te NWs D ~ 30–100 nm L ~ 3–10 μm	Te NWs D ~ 50–200 nm L ~ 3–10 μm	Sb-Te plates

The composition assessment is based on EDS except for the case of NPs synthesized using Sb and Te precursors. D, L and H represent mean diameter, length and/or thickness estimated from TEM images, respectively.

peaks show that all samples are composed of elemental Te with hexagonal phase (Fig. 3A-C). For detailed XRD peak assignment, see Supplementary Information Tables S6 and S7. The formation of elemental Te in all cases may occur because of the relatively high reduction potential of Te^{4+}, $E^{\circ}_{red}(Te^{4+}/Te) = 0.529$ V , which enhances the ability of Te to be reduced under the synthetic conditions. In addition, $E^{\circ}_{red}(Te^{4+}/Te)$ is significantly higher than those of Bi^{3+} [$E^{\circ}_{red}(Bi^{3+}/Bi) = 0.16$ V] and Sb^{3+} [$E^{\circ}_{red}(Sb^{3+}/Sb) = 0.212$ V].[34] This supports the favorable tendency of elemental Te particles to be formed under the various reaction conditions while Bi and Sb exhibit many cases where particles were not formed. The elemental Te NPs with various morphologies illustrates the effect of capping ligand identity. The use of OAM or OAC/OAM capping system led to the formation of very long wires which appear to grow from a central nucleation point in different directions (Figs. 3D, E, S1 and S2). This phenomenon is especially apparent when using OAC/OAM as a capping species, in Fig. 3E a NW cluster can be observed with a central nucleation point and tapered wires protruding out from the center of the cluster.

Changing the capping ligand to DT resulted in roughly spherical particles with a diameter of ~100 nm (Fig. 3F). However, the mean crystalline size of Te NPs was estimated to be around 41 nm from the full width at half-maximum of the (101) primary peak by the Scherrer formula, which is smaller than the size estimated from TEM images (ca. > 100 nm) suggesting that the NPs have a platelet morphology. For detailed XRD peak assignment, see Supplementary Information Table S8.

Study of bimetallic synthesis approach

To further study the general synthetic system, the analysis was expanded to include binary metallic precursors in the synthesis under otherwise identical conditions to the monometallic cases. The resulting variation in particle formation in terms of composition, morphology and structure reveals the complex nature of this system. The understanding of the interdependence of each metal precursor along with the organic capping ligands is important for controlling the properties of the resulting NPs. Each combination of two elemental precursors was used with different capping ligand systems including OAM, OAC/OAM or DT to study the effect on the final particle characteristics. The general results for these syntheses are summarized in Table 2.

Synthesis of Bi-Sb NPs

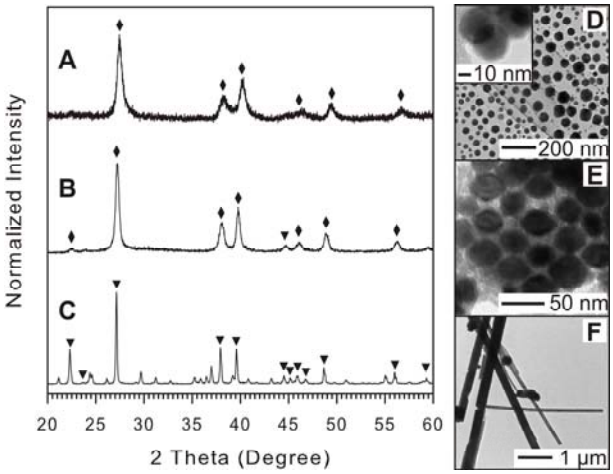

Fig. 4. XRD patterns and TEM images for Bi-Sb NPs synthesized using OAM (A and D), OAC/OAM (B and E), and DT (C and F). The identities of XRD peaks were labelled by filled diamond (♦) for Bi-Sb alloy (JCPDS card no. 00-035-0517) and filled triangle (▼) for Bi (JCPDS card no. 044-1246). For detail see Supplementary Information Tables S9-S11.

Bi-Sb materials were first synthesized using OAM, OAC/OAM and DT as capping systems. Figure 4 shows the XRD patterns and the corresponding TEM images collected for the three resulting materials with OAM (A, D and Fig. S6), OAC/OAM (B and E) and DT (C and F) capping system. When OAM is used, the particles appear roughly round (some particles are observed with hexagonal or pentagonal shape) with an approximate size of ~20–60 nm. However, in some places where particles overlap each other (the inset of Fig. 4D), we found that the overlapping areas were darker than the other areas which suggests NPs with a disc or platelet morphology. Additionally, the peaks in the XRD pattern for this sample (Fig. 4A) seems uncharacteristically broad (i.e. reflective of a smaller grain size), in light of these observations it may be that very thin platelets have formed in this synthesis approach. Weller and co-workers made a similar claim when they analyzed their $Bi_xSb_{2-x}Te_3$ nanoplatelets.[36] When OAC/OAM was used as a capping species, spherical and egg shaped NPs with a diameter around ~20–40 nm were obtained (Fig. 4E) with a morphology similar to Bi NPs formed in the monometallic synthesis using $BiCl_3$ and OAM or OAC/OAM (Fig. 1D). The broadened peaks appearing in the XRD pattern (Fig. 4B) arise as a result of the nanoscale size of the particles. The mean crystalline size of the NPs was calculated to be 19 nm from the full width at half-maximum of the (012) primary peak by the Scherrer formula, which is comparable with the size estimated from Fig. 4E as shown in Table 3 suggesting that the crystallinity of the NPs is quite good. For detailed XRD peak assignment, see Supplementary Information Tables S9 and S10. By analyzing the XRD peak positions in detail, all peaks are found to be in between the reference positions of pure Bi and Sb peaks for both samples. In addition, EDS analyses for the particles shown in Fig. 4D and E confirmed that the compositions of NPs are $Bi_{70}Sb_{30}$ and $Bi_{95}Sb_5$, respectively. Both Bi and Sb have a face-centered rhombohedral crystal structure, and they have complete solid solubility with each other[44] Early X-ray studies showed that the lattice parameter changes linearly with Sb concentration.[45] Hence, Vegard's law can be applied directly to

Table 3. Mean crystalline size calculated for NPs based on XRD pattern and Scherrer's formula

Metal Precursors	Capping Systems	Main Product	2 Theta (deg)	D_{XRD} (nm)	D_{TEM} (nm)
$TeCl_4$	DT	Te nanoplates	27.54	40.9	~ 100
$BiCl_3$, $SbCl_3$	OAM	BiSb nanoplates	27.45	14.6	39 ± 14
$BiCl_3$, $SbCl_3$	OAC/ OAM	BiSb NPs	27.28	19.0	32 ± 4
$BiCl_3$, $TeCl_4$	DT	BiTe NDs	27.62	43.1	~ 30–50
$SbCl_3$, $TeCl_4$	DT	SbTe plates	28.20	45.5	N/A

D_{XRD} and D_{TEM} represent mean crystalline size and NP size estimated from XRD patterns and TEM images, respectively.

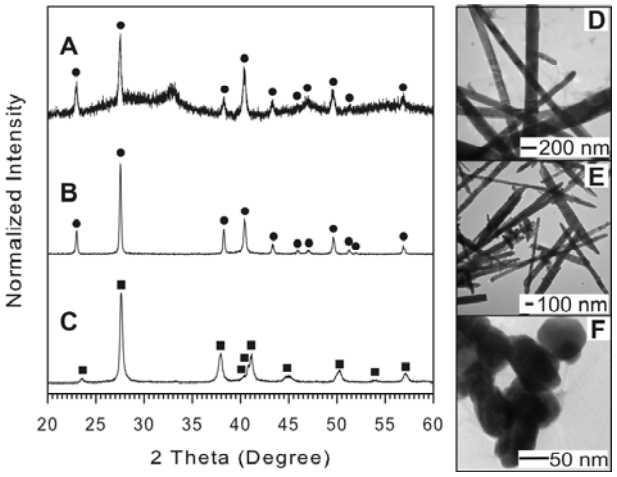

Fig. 5. XRD patterns and TEM images for Bi-Te materials synthesized using OAM (A and D), OAC/OAM (B and E), and DT (C and F). Filled circles (●) and filled squares (■) indicate peaks assigned for hexagonal-phase Te (JCPDS card no. 036-1452) and for rhombohedral Bi_2Te_3 (JCPDS card no. 015-0863), respectively. For detail see Supplementary Information Tables S12-S14.

the Bi-Sb alloy system. The mathematical expression of Vegard's law is given by

$$d_{BiSb} = xd_{Bi} + (100–x)d_{Sb} \quad (1)$$

where d_{Bi}, d_{Sb} and d_{BiSb} denote the lattice spacings of Bi, Sb and Bi_xSb_{100-x}, respectively, and x is the molar percent of Bi in the alloy. When the (012) lattice spacing (primary peaks in Fig. 4D and E) is plotted as a function of x, a clear linear relationship was obtained (Supplementary Information Fig. S7). As a result, it is concluded that both NPs synthesized using OAM and OAC/OAM as capping systems are Bi-Sb alloys with compositions of $Bi_{70}Sb_{30}$ and $Bi_{95}Sb_5$ respectively.

The formation of Bi-Sb solid solution NPs using OAM or OAC/OAM as capping systems without BiOCl suggests a bimetallic interaction in which Sb was first reduced, and then, Sb nuclei effectively catalyzed the decomposition and reduction of Bi precursor and/or Bi-ligand complex to form Bi-Sb solid solution NPs in light of the fact that BiOCl was a main product in the case of Bi monometallic synthesis (Fig. 1). In addition, the Bi-Sb NPs synthesized with the OAM capping system has a two-dimensional nanoplate shape while the NPs obtained in the Sb monometallic synthesis with the same capping system are one-dimensional NWs (Fig. 2C). This result indicates that the preferential growth directions of Bi-Sb and Sb are different from each other in the presence of the same capping ligand, OAM in this case.

On the other hand, the small spherical Bi-Sb NPs formed in the case of OAC/OAM capping system can be explained based on the improvement in the protecting ability of the double capping system. In combination, OAC and OAM were found to form the carboxylate anion with higher electron donating ability which is likely to result in a stronger interaction with the NP surface.[46] As a consequence of this stronger protection, the size of NPs becomes smaller as is the case in the Bi monometallic synthesis (small Bi NPs, see Fig. 1D). In addition, the lack of oxide and BiOCl peaks and the high Bi content in the NP composition in this case may arise as a result of the additional effect of Sb complex as a water scavenger due to the strong interaction of Sb with O in water,[47] effectively suppressing the formation of BiOCl. Furthermore, the adsorption and reduction of Bi complex at the Sb surface would explain the formation of Bi rich NPs instead of Sb NWs which were observed in the Sb monometallic synthesis using OAC/OAM.

Changing the capping ligand to DT, particles with elongated plate-like shape occur with a length of ~10 μm and diameter of ca. ~100–300 nm, along with some smaller spherical shaped NPs as shown in Fig. 4F. The XRD pattern reveals the formation of elemental Bi with some minor unidentifiable peaks as shown in Fig. 4C, which are characteristically the same pattern as those observed in Fig. 1C for monometallic Bi synthesized using DT (for detailed comparison see Supplementary Information Fig. S8). Therefore, these unidentifiable peaks could arise as a result of some by-product of bismuth and organic ligand that could not be removed in the particle purification process. One important observation is that there is no bismuth oxide or BiOCl peaks observed in the XRD pattern, which is consistent with the case of Bi monometallic synthesis using DT. The composition assessment using EDS shows only Bi without Sb in the final products. These results show the consistence with monometallic study for Bi and Sb with DT where Bi elongated plates grew and Sb-DT could not be reduced to form Sb NPs. This also suggests that once Bi is formed, it does not seem to catalyze the decomposition or reduction of the stable Sb-DT complex under the reaction conditions used here.

Synthesis of Bi-Te NPs

Figure 5 shows the XRD patterns (A-C) and TEM images (D-F) of NPs synthesized using $BiCl_3$ and $TeCl_4$ binary precursors. Figure 5D shows the TEM image of NPs synthesized using OAM capping system. As can be seen in Fig. 5D, NWs with a smooth surface and a relatively narrow diameter (~30–200 nm) with a length of several microns are obtained. Figure 5E shows that using OAC/OAM capping system leads to the formation of wire or bar shaped materials with a length of several microns and diameter of about ~100–200 nm. These wire shaped materials are mainly composed of elemental Te based on XRD analysis (Fig. 5A and B) and TEM-EDS measurement. The disappearance of Bi

in the final materials indicates that the alloying of Bi and Te did not occur and Te NWs did not promote the reduction of Bi complex to Bi under these synthetic conditions using OAM or OAC/OAM capping ligands. Moreover, BiOCl was not observed in the resulting synthesized material even though it was observed in the monometallic synthesis using OAM (Fig. 1A) or OAC/OAM (Fig. 1B). This may be due to the formation of a Te complex and preferential adsorption of the capping species on the Te NP surface (resulting in enhanced protection for Te NW during growth, effectively occupying a majority of the capping species). Therefore, BiOCl was not observed as a byproduct of the synthesis, or it may have been removed as a result of the washing process of the Te NPs after the synthesis.

TEM and XRD results for bimetallic NPs synthesized using DT capping species are given in Fig. 5C and F. From TEM images (Fig. 5F) captured for this sample, the NPs appear to be highly aggregated and have a disc-like morphology. The NPs are not uniform in size, but seem to be very thin as several particles can be observed that overlap each other. Some additional TEM images (Supplementary Information Fig. S9) collected for the resulting NPs show the varying image contrast caused by the different alignment of NDs to the electron beam where very light, roughly spherical NPs correspond to the top-down alignment and very dark rod like NPs offer a side view of the discs. The NDs have a diameter of about ~30–50 nm and thickness of about ~5–10 nm. The broad peaks in the XRD pattern (Fig. 5C) collected for these NPs may arise as a result of the nanoscale size and thin platelet morphology. Analysis of the composition based on assigning XRD peaks shows the presence of Bi_2Te_3 phase which is consistent with the fact that both Bi and Te particles were formed in the monometallic approach using DT.

The higher standard reduction potential of Te(IV) likely leads to an initial reduction and nucleation of Te followed by the reduction of Bi complex to form Bi_2Te_3. The Te particle surface in this case catalyzed the decomposition of the Bi complex followed by the alternate adsorption/reduction reaction of Bi and Te, resulting in the Bi_2Te_3 phase and ND morphology instead of Bi elongated plates as found for Bi synthesized with DT (Fig. 1E). The formation of Bi_2Te_3 NDs capped with DT arises primarily as a result of the catalytic effect of Te at the particle surface in the decomposition of the Bi-DT complex which introduces an intriguing pathway to modify the final NP morphology and composition.

Synthesis of Sb-Te NPs

Figure 6 shows the XRD patterns (A-C) and TEM images (D-F) of NPs synthesized using $SbCl_3$ and $TeCl_4$ binary precursors. It was found that the synthesis using $SbCl_3$ and $TeCl_4$ with OAM or OAC/OAM capping systems resulted in the formation of NWs (Fig. 6D and E) with a length of several microns and diameter of about ~30–200 nm. The XRD peak assignment (Fig. 6A and B) for these materials indicates the formation of only elemental Te without any sign of Sb or other compounds which is in agreement with EDS analysis. It seems that Sb was not reduced or incorporated into the Te NWs even though both Sb and Te NWs can be created using these two capping systems in monometallic syntheses. From the study of Sb-DT complex, the complex fragments are noted to have very high molecular weight (Supplementary Information Fig. S4) which may reflex the fact that several capping ligand species are required to form the

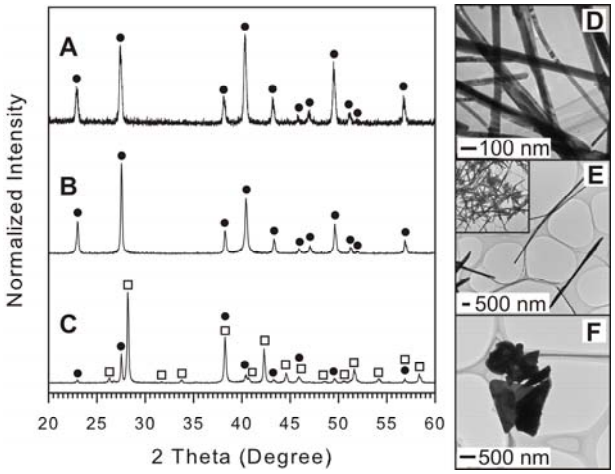

Fig. 6. XRD patterns and TEM images for Sb-Te materials synthesized using OAM (A and D), OAC/OAM (B and E), and DT (C and F). The peak identities were labelled by the symbol filled circle (●) for Te (JCPDS card no. 036-1452) and open square (□) for Sb_2Te_3 (JCPDS card no. 015-0874). The inset of Fig. 6E represents a zoomed out view of synthesized NWs. For detail see Supplementary Information Tables S15-S17.

complex. Therefore, in bimetallic synthesis when the amount of capping ligands used in the synthesis is double the normal amount, there still may not be a sufficient amount to make a stable complex with all metal precursors. The lack of Sb in the resulting NWs can be explained due to the fact that most capping species were used to make the complex with Te and were adsorbed on the Te NW surface rather than making a complex with $SbCl_3$. As a result, $SbCl_3$ or even Sb oxide and other compounds, such as SbOCl, would likely be removed in the particle washing process.

Using DT as a capping system, on the other hand, leads to the formation of large platelet-like particles (Fig. 6F) composed of Sb_2Te_3 with a minor amount of elemental Te as indexed in the XRD pattern (Fig. 6C). The formation of two segregated phases including Sb_2Te_3 and Te indicates that the existence of Te NPs catalyzed the decomposition and reduction of the Sb-DT complex, which failed to be reduced in the Sb monometallic synthesis with DT (see Table 1).

Summary of the mono- and bi-metallic synthesis studies

From the study of mono- and bi-metallic syntheses, we can elucidate the role that each individual capping ligand plays, as well as the influence of the metallic interaction in the formation of the NPs. The formation of NPs is summarized for two general types of capping systems: one is DT and the other is OAM and OAC/OAM. For the first case, DT creates a relatively strong complex with the three elemental precursors, especially with Sb which could not be reduced in the monometallic synthesis. The resulting small Te nanoplates and long Bi particles without oxides and other compounds in single precursor approach show the good capping ability of DT. Furthermore, the results of the bimetallic system capped with DT highlighted the important catalytic effect of Te for Bi_2Te_3 and Sb_2Te_3 formation. We also found that NPs composed of Bi and Sb failed to be formed in DT due to the stability of Sb-DT complex along with no catalytic effect of Bi particles. Therefore, the strong bimetallic interaction

of Te with Bi and/or Sb-DT complexes and the lack of Bi-Sb alloy formation explain the existence of two segregated phases obtained when using DT with all three elemental precursor synthesis.[37] On the other hand, OAM or OAC/OAM, in the interaction with single precursor, directs the growth of monoelemental Sb and Te NWs as well as the BiOCl formation with a minor phase of Bi. In these capping systems, if Te does not act as catalyst for Bi or Sb complex reduction, then only monometallic Te NWs grow in the bimetallic systems. However, Bi and Sb can be incorporated into a Bi-Sb alloy NP as a result of the formation and catalytic effect of Sb on the Bi complex. Therefore, in OAM or OAC/OAM capping systems, there is a possibility of forming a $(Bi,Sb)_2Te_3$ ternary solid solution when all three elemental precursors are combined together. The general understanding of the NP formation mechanism encourages a study of the synthesis of trimetallic NPs using these capping species, toward $(Bi,Sb)_2Te_3$ ternary solid solution NPs.

Study of trimetallic synthesis approach

In light of the key results obtained from the formation mechanism investigation for monometallic and bimetallic syntheses, we synthesized trimetallic NPs with the OAM capping ligand system. In this section, the OAM capping system was focused on because of the failure to synthesize Bi-Sb alloy using DT capping system in the bimetallic synthesis, while only Bi-Te and Sb-Te alloys could be obtained using DT. Based on these results, it is likely that $Te/Bi_2Te_3/Sb_2Te_3$ segregated NPs would be dominantly synthesized if DT was used in a Bi-Sb-Te trimetallic synthesis. In fact, a similar result was previously reported in which phase-segregated NDs were obtained.[37] Therefore, the formation mechanism in this case is relatively simple, i.e., Te NP formation followed by Bi and Sb individual incorporation into the Te NPs due to the catalytic effect of Te without Bi-Sb interaction. Accordingly, it seems quite difficult to synthesize nanostructured $(Bi,Sb)_2Te_3$ solid solution using DT as a capping system. On the contrary, in the case of Bi-Sb bimetallic synthesis using OAM capping system, we successfully synthesized $Bi_{70}Sb_{30}$ alloy nanoplates, while Bi-Te and Sb-Te alloys could not be obtained using OAM. It is worthwhile to investigate whether a Bi-Sb-Te cross interaction takes place. The main results and discussion of this section, therefore, will detail only trimetallic NWs synthesized with OAM capping species which give more insight into the growth mechanism of Bi-Sb-Te NPs and how to control the resulting shape, composition and structure.

Using OAM as a capping ligand led to the formation of very long and high aspect ratio NWs. Figure 7 shows the TEM images of NWs synthesized using 0.17 mL OAM (corresponding to 1:1 molar ratio of elemental precursors to OAM). The length of the NWs is several microns with a diameter ranging from 50 to 100 nm, which gives a very high aspect ratio (~50–100). On the surface of the NWs, there are some small NPs and the non-homogeneous local areas (reflected by different contrast) observed in the TEM images for each NW may indicate a heterogeneous composition. In addition, if one takes a close look at Fig. 7C, the center of a NW is lighter than the periphery suggesting the composition distribution in a radial direction (i.e. Bi-rich at the periphery) or the tube-like structure caused by nanoscale Kirkendall effect[31] which refers to a nonreciprocal mutual diffusion through an interface of two metals. HRTEM

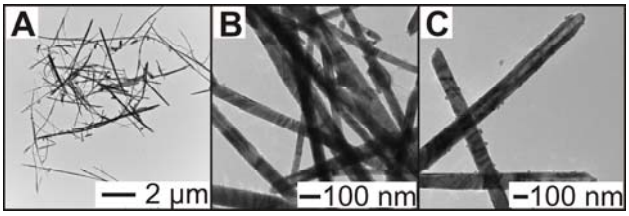

Fig. 7. TEM images of trimetallic NWs synthesized using OAM as capping species with 1:1 molar ratio of precursors and OAM. Image (A) shows the zoomed out view of the synthesized NWs, (B) shows a magnified view of the NWs which have a narrow diameter and are smooth, and (C) shows NWs with some smaller NPs at the surface and the tip of NWs.

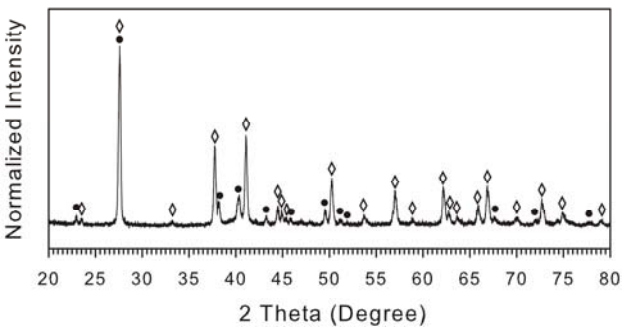

Fig. 8. XRD patterns of trimetallic NWs synthesized using OAM as capping species with 1:1 molar ratio of precursors and OAM. The peak identities are labelled by the symbol filled circle (●) for Te (JCPDS card no. 036-1452), and open diamond (◊) for $(Bi_{0.5}Sb_{0.5})_2Te_3$ (JCPDS card no. 01-072-1835).

images of a single NW is shown in Fig. S10, illustrating the high crystallinity of particles. The composition and crystal structure of the NWs was analyzed using ICP-MS and XRD.

Figure 8 shows the XRD patterns for NWs capped with OAM. XRD peaks can be indexed for several segregated phases including Te (hexagonal structure), Bi_2Te_3, and $(Bi,Sb)_2Te_3$ (rhombohedral structure) due to their similar crystal structures and overlapping peaks. The reference reflection of bulk $(Bi_{0.5}Sb_{0.5})_2Te_3$ was used to assign the peak position of $(Bi,Sb)_2Te_3$ phase. Note that Sb_2Te_3, Sb or Sb oxide phases could not be found in the XRD pattern. To assign the phases definitively, the elemental assessment for NWs using ICP-MS analysis was conducted with the results of $Bi_{15}Sb_{26}Te_{59}$, which is in general consistent with each other in the co-existence of all three metal components. Note that the accurate elemental assessment of Bi-Sb-Te ternary material is difficult using EDS because Sb and Te peaks overlap each other significantly. We conclude that dominant phases of the NWs synthesized using OAM capping system are $(Bi,Sb)_2Te_3$ (rhombohedral) and elemental Te (hexagonal) by considering the following facts: 1) the NWs have no Sb_2Te_3, Sb or Sb oxide phases, 2) the NWs contain a significant amount of Sb, and 3) the presence of the characteristic peaks of Te at 2θ = 22.98, 38.21, 40.38, 43.28, 49.55, 51.16, and 51.92 degrees and of $(Bi,Sb)_2Te_3$ at 2θ = 70.06 degrees. Note that we do not rule out the existence of Bi_2Te_3 phase because other peaks of $(Bi,Sb)_2Te_3$ phase significantly overlap with Bi_2Te_3 phase. For detail see Supplementary Information Table S18.

Summary of the nanoparticle formation mechanism

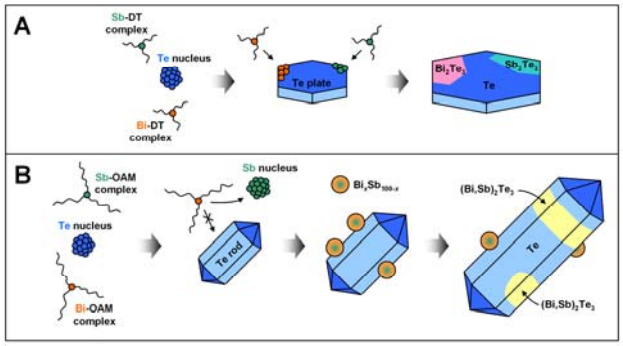

Fig. 9. Schematic illustration of formation mechanisms for (A) $Te/Bi_2Te_3/Sb_2Te_3$ phase-segregated NDs synthesized using DT as a capping system and for (B) $Te/(Bi,Sb)_2Te_3$ NWs synthesized using OAM as a capping system.

To consistently explain all the results in the systematic studies about the effect of capping ligands and metal complex interaction on NP morphology and composition, we propose two separate formation mechanisms for BiSbTe containing NPs with two kinds of capping systems: OAM and DT based on the metal-ligand complex formation, decomposition and interaction. In general, due to the high reduction potential, Te complex was first reduced, undergoing nucleation. However, the growth of Te NPs and the incorporation of other metals strongly depend on the capping ligands (formation of complex with the metal precursors) and the metal-ligand cross-interaction.

In the case for DT, a stable complex with Sb can be formed, with a less stable complex for Bi or Te. As a result, the Sb-DT complex itself could not be reduced under the synthetic conditions, but Bi and Te can be reduced and form elongated plates or nanoplates respectively. Bi was not found to catalyze the reduction of the Sb-DT complex, as indicated in the bimetallic approach which led to the formation of only monometallic Bi plates. On the other hand, Te NDs could act as a catalyst for Bi or Sb complex reduction, resulting in the formation of Bi_2Te_3 and Sb_2Te_3 materials. The existence of these two phases in trimetallic NPs synthesized using DT therefore can be explained based on the catalytic effect of Te and reaction of Te with the other metal complexes.

When OAM is used as a capping system, Te does not exhibit catalytic properties in the reduction of the other metal complexes. Moreover, the formation of Te containing NWs for all synthesis approaches with the presence of Te precursor and OAM indicated that the growth of Te NWs capped with OAM is preferential and the incorporation of other metals into the NWs is not feasible when using OAM. In this capping system, Sb was found to play a dual role in catalyzing the decomposition of the Bi complex, which prevented the formation of BiOCl. It is very important that a Bi-Sb alloy can be formed under similar synthetic conditions with OAM. The formation of these materials illustrates the possibility to form an alloy of BiSbTe when all three metal precursors are used in the synthesis. Therefore, the reduction and growth of Te NWs and Bi-Sb NPs can occur separately in the trimetallic synthesis, and the formation of the final NWs containing $(Bi,Sb)_2Te_3$ ternary solid solution may be caused by the oriented attachment[42] of Te NWs and Bi-Sb NPs which was not observed in the case of using DT as capping ligand. The formation mechanism in these two cases is illustrated in Fig. 9.

Conclusions

In conclusion, we have partially addressed the complexity in the growth mechanism of trimetallic nanoparticles based on the synthesis and investigation of monometallic and bimetallic systems using various capping ligands. The use of different capping ligands in the complex formation and metallic interaction result in two different pathways in the formation of trimetallic NPs. Our study illustrates the formation of Bi_2Te_3 and Sb_2Te_3 based NPs due to the Te catalytic effect on the decomposition of the Sb and Bi precursor complexes. A bimetallic interaction was also observed in the case of using DT capping species. The formation of BiSb alloy in the OAM based capping system is important for the formation of a trimetallic alloy, which is observed in the triple elemental synthetic approach. The understanding of the NP formation mechanism arising from this expansive study gives a fundamental understanding of how to further control the composition, structure and characteristics of trimetallic NPs towards TE materials with enhanced and promising properties. Part of the ongoing work includes further delineation of the synthetic parameters, including precursor concentrations as well as characterization of the TE properties of these materials.

Acknowledgment

This work was supported by the Grant-in-Aid for Scientific Research (C). Nguyen T. Mai would like to thank the Vietnamese Government for a 322 scholarship. We thank Drs. M. Koyano and K. Suekuni from JAIST for valuable advice and discussion.

Notes and references

School of Materials Science, Japan Advanced Institute of Science and Technology (JAIST), 1-1 Asahidai, Nomi, 923-1292, Japan. Fax: +81-761-51-1625; Tel:+81-761-51-1611; E-mail:shinya@jaist.ac.jp (S. M.)

† Electronic Supplementary Information (ESI) available: SEM and HRTEM images of Sb and Te NWs, XRD peak assignments for all samples, photographs of metal-ligand complexes, FTICR-MS spectrum and TGA data of Sb-DT complex, HRTEM image of BiSb NPs, relationship between lattice spacing and composition of BiSb alloy, comparison of XRD peak position collected for NPs synthesized using $BiCl_3$ and $BiCl_3/SbCl_3$ with DT as capping ligands, bimetallic synthesis of Bi-Te halide precursors and DT, HRTEM images of a single Bi-Sb-Te NW, and results for trimetallic approach using oleic acid as capping system. See DOI: 10.1039/b000000x/

1 G. J. Snyder and E. S. Toberer, *Nat. Mater.*, 2008, **7**, 105.
2 *Thermoelectrics Handbook: Macro to Nano*; D. M. Rowe, Ed.; CRC Press: Boca Raton, FL, 2006.
3 M. V. Kovalenko, B. Spokoyny, J.-S. Lee, M. Scheele, A. Weber, S. Perera, D. Landry and D. V. Talapin, *J. Am. Chem. Soc.*, 2010, **132**, 6686.
4 Y.-M. Lin and M. S. Dresselhaus, *Phys. Rev. B*, 2003, **68**, 075304.
5 B. Yoo, F. Xia, K. N. Bozhilov, J. Herman, M. A. Ryan and N. V. Myung, *Adv. Mater.*, 2007, **19**, 296.
6 A. E. Saunders, A. Ghezelbash, D.-M. Smilgies, M. B. Sigman and B. A. Korgel, *Nano Lett.*, 2006, **6**, 2959.
7 R. Venkatasubramanian, E. Siivola, T. Colpitts and B. O'Quinn, *Nature*, 2001, **413**, 597.
8 Y. Zhao, J. S. Dyck, B. M. Hernandez and C. Burda, *J. Phys. Chem. C*, 2010, **114**, 11607.
9 Y. Q. Cao, T. J. Zhu, X. B. Zhao, X. B. Zhang and J. P. Thu, *Appl. Phys. A: Mater. Sci. Process*, 2008, **92**, 321.

10 S. H. Li, M. S. Toprak, H. M. A. Soliman, J. Zhou, M. Muhammed, D. Platzek and E. Muller, *Chem. Mater.*, 2006, **18**, 3627.
11 S. H. Li, H. M. A. Soliman, J. Zhou, M. S. Toprak, M. Muhammed, D. Platzek, P. Ziolkowski and E. Muller, *Chem. Mater.*, 2008, **20**, 4403.
12 F. Xiao, C. Hangarter, B. Yoo, Y. Rheem, K.-H. Lee and N. V. Myung, *Electrochim. Acta*, 2008, **53**, 8103.
13 H. Ebe, M. Ueda and T. Ohtsuka, *Electrochim. Acta*, 2007, **53**, 100.
14 A. Bailini, F. Donati, M. Zamboni, V. Russo, M. Passoni, C. S. Casari, A. L. Bassi and C. E. Bottani, *Appl. Surf. Sci.*, 2007, **254**, 1249.
15 C. N. Liao, K. M. Liou and H. S. Chu, *Appl. Phys. Lett.*, 2008, **93**, 042103.
16 S. S. Kim, S. Yamamoto and T. Aizawa, *J. Alloys Compd.*, 2004, **375**, 107.
17 X. A. Fan, J. Y. Yang, R. G. Chen, W. Zhu and S. Q. Bao, *Mater. Sci. Eng. A*, 2006, **438**, 190.
18 J. L. Cui, H. F. Xue, W. J. Xiu, L. Jiang and P. Z. Ying, *J. Solid State Chem.*, 2006, **179**, 3751.
19 T.-S. Kim and B.-S. Chun, *J. Alloys Compd.*, 2007, **437**, 225.
20 R. J. Mehta, C. Karthik, W. Jiang, B. Singh, Y. Shi, R. W. Siegel, T. Borca-Tasciuc and G. Ramanath, *Nano Lett.*, 2010, **10**, 4417.
21 R. J. Mehta, C. Karthik, B. Singh, R. Teki, T. Borca-Tasciuc and G. Ramanath, *ACS Nano*, 2010, **4**, 5055.
22 X. F. Qiu, C. Burda, R. L. Fu, L. Pu, H. Y. Chen and J. J. Zhu, *J. Am. Chem. Soc.*, 2004, **126**, 16276.
23 W. Wang, J. Goebl, L. He, S. Aloni, Y. Hu, L. Zhen and Y. Yin, *J. Am. Chem. Soc.*, 2010, **132**, 17316.
24 Y. Xu, Z. Ren, G. Cao, W. Ren, K. Deng and Y. Zhong, *Mater. Lett.*, 2008, **62**, 4525.
25 Y. Deng, C.-W. Nan, G.-D. Wei, L. Guo and Y. Lin, *Chem. Phys. Lett.*, 2003, **374**, 410.
26 W. Lu, Y. Ding, Y. Chen, Z. L. Wang and J. Fang, *J. Am. Chem. Soc.*, 2005, **127**, 10112.
27 A. Purkayastha, S. Kim, D. D. Gandhi, P. G. Ganesan, T. Borca-Tasciuc and G. Ramanath, *Adv. Mater.*, 2006, **18**, 2958.
28 A. Scheele, N. Oeschler, K. Meier, A. Kornowski, C. Klinke and H. Weller, *Adv. Funct. Mater.*, 2009, **19**, 3476.
29 J.-J. Kim, S.-H. Kim, S.-W. Suh, D.-U. Choe, B.-K. Park, J. R. Lee and Y.-S. Lee, *J. Cryst. Growth*, 2010, **312**, 3410.
30 A. Purkayastha, Q. Y. Yan, M. S. Raghuveer, D. D. Gandhi, H. F. Li, Z. W. Liu, R. V. Ramanujan, T. Borca-Tasciuc and G. Ramanath, *Adv. Mater.*, 2008, **20**, 2679.
31 G. Zhang, Q. Yu, Z. Yao and X. Li, *Chem. Commun.*, **2009**, 2317.
32 J. Yang, T. Aizawa, A. Yamamoto and T. Ohta, *J. Alloys Compd.*, 2000, **309**, 225.
33 J. Jiang, L. Chen, S. Bai, Q. Yao and Q. Wang, *J. Cryst. Growth*, 2005, **277**, 258.
34 Y. Xu, Z. Ren, W. Ren, K. Deng and Y. Zhong, *Mater. Lett.*, 2008, **62**, 763.
35 Y. Zhao and C. Burda, *ACS Appl. Mater. Interf.*, 2009, **1**, 1259.
36 M. Scheele, N. Oeschler, I. Veremchuk, K.-G. Reinberg, A.-M. Kreuziger, A. Komowski, J. Broekaert, C. Klinke and H. Weller, *ACS Nano*, 2010, **4**, 4283.
37 D. Mott, N. T. Mai, N. T. B. Thuy, Y. Maeda, T. P. T. Linh, M. Koyano and S. Maenosono, *Phys. Status Solidi A*, 2011, **208**, 52.
38 Z. Liu, Z. Hu, J. Liang, S. Li, Y. Yang, S. Peng and Y. Quian, *Langmuir*, 2004, **20**, 214.
39 S. Saita and S. Maenosono, *Chem. Mater.*, 2005, **17**, 6624.
40 D. D. Fanfair and B. A. Korgel, *Cryst. Growth Des.*, 2008, **89**, 3246.
41 J.-L. Mi, N. Lock, T. Sun, M. Christensen, M. Søndergaard, P. Hald, H. H. Hng, J. Ma and B. B. Iversen, *ACS Nano*, 2010, **4**, 2523.
42 Y. Deng, C. W. Nan and L. Guo, *Chem. Phys. Lett.*, 2004, **383**, 572.
43 R. Malakooti, L. Cademartiri, Y. Akcakir, S. Petrov, A. Migliori and G. A. Ozin, *Adv. Mater.*, 2006, **18**, 2189.
44 A. M. Ibrahim and D. A. Thompson, *Mater. Chem. Phys.*, 1985, **12**, 29.
45 W. F. Ehret and M. B. Abramson, *J. Am. Chem. Soc.*, 1934, **56**, 385.
46 Y. Li and J. Liu, *Chem. Mater.*, 2001, **13**, 1008.
47 K. A. Abboud, R. C. Palenik and R. M. Wood, *Inorg. Chim. Acta*, 2007, **360**, 3642.

